AD-A268 067

DOCUMENTATION PAGE

Form Approved
OMB No. 0704-0188

DTIC
ELECTE
AUG 6 1993
S C D

1a. SECURITY CLASSIFICATION AUTHORITY	1b. RESTRICTIVE MARKINGS
2b. DECLASSIFICATION / DOWNGRADING SCHEDULE	3. DISTRIBUTION / AVAILABILITY OF REPORT DISTRIBUTION STATEMENT A Approved for public release
4. PERFORMING ORGANIZATION REPORT NUMBER(S)	5. MONITORING ORGANIZATION REPORT NUMBER(S)
6a. NAME OF PERFORMING ORGANIZATION Dept. of Aerospace Engineering and Engineering Mechanics	6b. OFFICE SYMBOL (If applicable)
6c. ADDRESS (City, State, and ZIP Code) The Univ. of Texas at Austin Austin, TX 78712-1085	7a. NAME OF MONITORING ORGANIZATION ONR 7b. ADDRESS (City, State, and ZIP Code)
8a. NAME OF FUNDING / SPONSORING ORGANIZATION ONR	8b. OFFICE SYMBOL (If applicable)
8c. ADDRESS (City, State, and ZIP Code) Office of Naval Research/Code 1132P 800 N. Quincy Street Arlington, VA 22217-5000	9. PROCUREMENT INSTRUMENT IDENTIFICATION NUMBER Grant No. N00014-91-J-1738

10. SOURCE OF FUNDING NUMBERS

PROGRAM ELEMENT NO.	PROJECT NO.	TASK NO.	WORK UNIT ACCESSION NO.
	4326814-02		

11. TITLE (Include Security Classification)

Damage Evolution in Filled Elastomers

12. PERSONAL AUTHOR(S)

K. Ha, S. Park and R. A. Schapery

13a. TYPE OF REPORT	13b. TIME COVERED	14. DATE OF REPORT (Year, Month, Day)	15. PAGE COUNT
FINAL	FROM 10/90 TO 3/93	1993, June, 17	

16. SUPPLEMENTARY NOTATION

17. COSATI CODES			18. SUBJECT TERMS (Continue on reverse if necessary and identify by block number)
FIELD	GROUP	SUB-GROUP	Solid Propellant, Viscoelasticity, Damage Growth, Crack Growth.

19. ABSTRACT (Continue on reverse if necessary and identify by block number)

This report summarizes theoretical and experimental research on distributed damage growth and its effect on stress-strain behavior and on the strain distribution around macro-cracks in particle-filled rubber. Two Appendices provide details on the constitutive model, experimental determination of deformation and damage in specimens under axial straining and confining pressure, and experimental measurement of strain fields in biaxially-stressed specimens with cracks.

93 6 28 054

93-18786

20. DISTRIBUTION / AVAILABILITY OF ABSTRACT	21. ABSTRACT SECURITY CLASSIFICATION
☐ UNCLASSIFIED/UNLIMITED ☐ SAME AS RPT. ☐ DTIC USERS	
22a. NAME OF RESPONSIBLE INDIVIDUAL Dr. Richard L. Miller, Code 1132P	22b. TELEPHONE (Include Area Code) (703) 696-4405
	22c. OFFICE SYMBOL

DD Form 1473, JUN 86 Previous editions are obsolete. SECURITY CLASSIFICATION OF THIS PAGE

unclassified

93 8 11 029

DISCLAIMER NOTICE

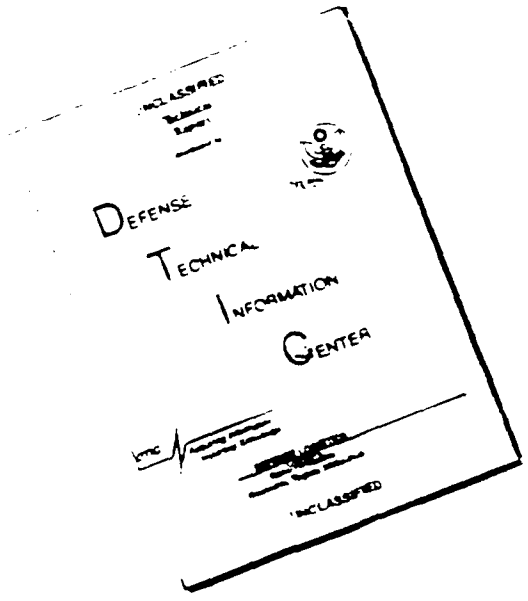

THIS DOCUMENT IS BEST QUALITY AVAILABLE. THE COPY FURNISHED TO DTIC CONTAINED A SIGNIFICANT NUMBER OF PAGES WHICH DO NOT REPRODUCE LEGIBLY.

SUMMARY OF WORK ACCOMPLISHED

The research consisted primarily of two distinct but related studies of particle-filled rubber: 1. distributed damage growth and deformation behavior and 2. macrocracking in a composite with distributed, growing damage. Two Ph.D. students, Mr. Sunwoo Park (study No. 1) and Mr. Kuendong Ha (study No. 2) participated in the research, under the direction of Professor R. A. Schapery. The test material was an inert solid propellant provided by the Naval Weapons Center.

This summary is divided into discussion of these two areas in Sections 1 and 2 below. For each, a brief, general summary is given. Work that has not yet been published is described in related Appendices. Otherwise, reference to publications is made. Work that was published during the period of this grant is listed in Section 3 as part of this summary. A separate list of references then follows; this list contains all publications that are referenced in the Summary and the Appendices. The research is continuing as part of the two students' Ph.D. degree requirements.

1 Damage Growth and Deformation Behavior

The objective of this part of the project was to predict damage growth (distributed microcracking) and establish a nonlinear thermoviscoelastic constitutive equation for a highly filled rubber with effects of damage. A work potential theory presented by Schapery (1990), a simplification scheme (Schapery 1991a), and a micromechanical model (Schapery 1991b) were combined to serve as the basis for the development of the present model. Several series of mechanical tests have been performed to provide data for model characterization and verification.

A theory based on thermodynamics with internal state variables was developed previously by Schapery (1990) to describe the mechanical behavior of elastic and viscoelastic media with growing damage. The theory has been found to successfully characterize and predict the *elastic* mechanical behavior of particulate- and fiber-reinforced composites with changing internal structure. However, except for certain theoretical idealizations, effects of *viscoelasticity and temperature* were not explicitly considered in these applications. Therefore, the current project was undertaken to refine the theory to cover realistic behavior in these areas and to assess its validity through an experimental study of particle-reinforced rubber.

A combination of a gas dilatometer, an Instron universal testing machine, and an environmental chamber was used to measure the stresses and dilatations of bar-shaped test specimens subjected to axial straining with different strain rates, confining pressures, and

temperatures. A moderate-elongation inert solid propellant produced by the Naval Weapons Center was employed as the test material. JANNAF Class-A uniaxial specimens were used. An automated data acqusition system on a personal computer was employed. Further details of the theory and experiments are provided in Appendix A.

2 Macrocracking with Distributed, Growing Damage

The effect of macrocrack in particle-filled rubber has been investigated. The results for a linear elastic behavior of a biaxially stressed strip with a through center-crack was obtained using a finite element model (ABAQUS). The micromechanical model which accounts for effects of microcracking (described in the Appendix A) is to be incorporated into the finite element method with user defined potentials like strain energy. In order to study this problem in detail and validate the theory which accounts for distributed damage, it was decided to develop an experimental technique capable of measuring local displacements in the biaxial strip specimen. Description of the experimental method is in Appendix B. In summary, first a grid was applied on the specimens for in-plane, two-dimensional displacement measurements. A second and better method based on the cross-correlation of digital images was used and demonstrated for acquiring displacement distributions. Details of both methods are given in Appendix B. Where there is not significant distributed damage, the experimental results closely agreed with theoretical results from linear theory and partially confirm measurements of others (T.C.Chu, 1985). Further improvement of resolution and accuracy of the second measurement technique, as well as application of the constitutive model with damage (described in Appendix A) in predicting solutions of boundary-value problems in media with macrocracks, are planned.

3 Articles Published During Grant Period

Papers Numbers 1 and 2 provide the main basis for the theoretical modeling and experimental work on this project. Papers Numbers 3 and 4 summarize relevant research results on the present and earlier grants and describe a method for selecting particle-size distributions which minimize microcracking due to mechanical loading.

1. Schapery, R. A., "Simplifications in the Behavior of Viscoelastic Composites with Growing Damage," Proc. IUTAM Symposium on *Inelastic Deformation of Composite Materials*, (G. J. Dvorak, Ed.), Springer, New York, pp. 193–214 (1991).

2. Schapery, R. A., "Analysis of Damage Growth in Particulate Composites Using a Work Potential," *Composites Engineering*, Vol. 1, pp. 167–182 (1991).

3. Schapery, R. A., "Cracking in Viscoelastic Propellants," Proc. ONR Workshop on *Desensitization of Explosives and Propellants*, TNO Prins Maurits Laboratory, Delft, (No. 11-13, 1991).

4. Schapery, R. A., "Damage Growth in Composite Propellants," Proc. ONR/LANL Workshop on *Fundamental Physics and Chemistry of Combustion, Initiation, and Detonation of Energetic Materials*, Los Alamos National Laboratory, (March 3-6, 1992).

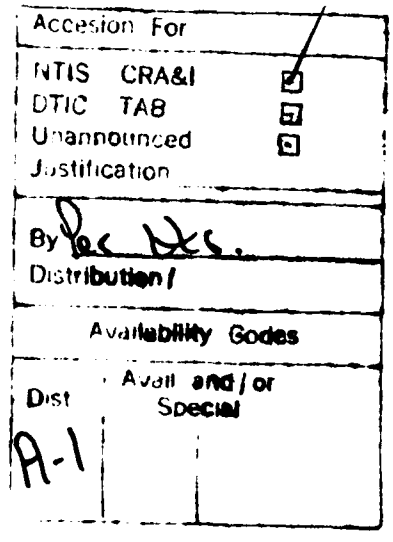

REFERENCES

Boggs, T. L., Price, C. F., Richter, H. P., Atwood, A. I., Lepie, A. H., Zwierzchowski, N. G., and Boyer, L. R., 1988, "Detonation of undamaged and damaged energetic materials," *Combustion and Detonation Phenomena*, (Proc. 19th Int'l Annual Conference of ICT), 30-1 to 30-13.

Chu, T.C., et. al., 1985, "Applications of Digital-Image-Correlation Techniques to Experimental Mechanics," *Journal of Experimental Mechanics*, 232.

Farris, R. J., 1968, "The character of the stress-strain function for highly filled elastomers," *Tran. Soc. Rheology*, **12(2)**, pp. 303–314.

Farris, R. J., 1983, "Mechanical behavior and dilatation of particulate-filled thermosets in the rubbery state," *Journal of Applied Polymer Science*, **28**, pp. 3369–3386.

Franke, E.A., Wenzel, D.J., and Davidson, D.L., 1991, "Measurement of Microdisplacements by Machine Vision Photogrammetry," *Rev. Sci. Instrum.*, **62(5)**, pp. 1270-1276.

Hufferd, W. L., 1980, "Thermal-mechanical interaction in filled polymers," *Proc. of the NSF Workshop on A Continuum Mechanics Approach to Damage and Life Prediction*, Carrollton, Ky.

Mullins, L., 1969, "Softening of rubber by deformation," *Rubber Chem Technol*, **42**, pp. 339-362.

Peng, S.T.J., 1985, "Nonlinear multiaxial finite deformation investigation of solid propellants," Air Force Rocket Propulsion Laboratory Report AFRPL- TR-84-036.

Post, D., Smith, C.W., and Czarnek, R., 1987, "Crack Opening and Extension in Inert Solid Propellant – An Experimental Study," Final Report prepared for the Air Force Astronautics Laboratory.

Schapery, R. A., 1974, "A nonlinear constitutive theory for particulate composites based on viscoelastic fracture mechanics," *Proc. of the 11th Meeting of the JANNAF Structures & Mechanical Behavior Working Group, Chemical Propulsion Information Agency*, Publication No. 253.

Schapery, R. A., 1978, "Mechanical behavior of solid propellant," ONR Workshop on *Deflagration-to-Detonation Transition.*

Schapery, R. A., 1982, "Models for damage growth and fracture in nonlinear viscoelastic particulate composites," *Proc. Ninth U.S. National Congress of Applied Mechanics*, Book No. H00228 (Edited by Y, H, Pao), ASME, New York, pp. 237—245.

Schapery, R. A., 1986, "A micromechanical model for nonlinear viscoelastic behavior of particle-reinforced rubber with distributed damage," *Eng'g Fracture Mechanics*, **25**, pp. 845–867.

Schapery, R. A., 1989, "Mechanical characterization and analysis of inelastic composite laminates with growing damage," *Mechanics of Composite Materials and Structures*, ASME AMD-Vol 100, pp. 1–9.

Schapery, R. A., 1990, "A theory of mechanical behavior of elastic media with growing damage and other changes in structure," *J. Mech Phys Solids*, **38**, pp. 215–253.

Schapery, R. A., 1991a, "Simplifications in the behavior of viscoelastic composites with growing damage," *Proc IUTAM Symposium on Inelastic Deformation of Composite Materials*, Troy, New York, (Edited by G. J. Dvorak), Springer, New York-Wien, pp. 193–214.

Schapery, R. A., 1991b, "Analysis of Damage Growth in Particulate Composites Using a Work Potential, *Composites Engineering*, **1**, pp. 167–182.

Simo, J. C., 1987, "On a fully three-dimensional finite strain viscoelastic damage model: formulation and computational aspects," *Computer Methods in Appl Mech and Eng'g*, **60**, pp. 153–173.

Swanson, S. R., and Christensen, L. W., 1983, "A constitutive formulation for high-elongation propellants," *J. Spacecraft Rockets* , **20**, pp. 559–566.

APPENDIX A
Damage Growth and Deformation Behavior

Introduction

Reduction of hazard sensitivities of energetic materials, such as solid propellant, has long been sought. Studies have shown that void volume has a major effect on the sensitivity of energetic materials (Boggs et.al. 1988). Whether these voids are due to mechanical deformation, poor processing, or aging at high temperatures or humidities, they enhance susceptibility to detonation from shock or deflagration.

The mechanisms of initiation and growth of microvoids in solid propellant under mechanical loading are relatively well defined (e.g., Schapery 1978, Boggs et.al. 1988). A widely used solid propellant is a particulate composite which consists of hard particles and rubber matrix. When such a particulate composite material is deformed, high triaxial stress concentrations develops in the binder near the surface of each filler particle. Vacuole formation is believed to initiate when this stress exceeds some critical value. If hydrostatic pressure is applied while the material is deformed, the pressure will retard vacuole formation. It has been observed that vacuole formation is accelerated with increasing strain rate.

A series of tests has been performed to characterize the deformation behavior and to quantify the vacuole formation of an inert solid propellant. The specimens were subjected to axial straining under a fixed hydrostatic pressure. Different strain rates, pressures, and temperatures were applied to each specimen. The material used in the research is an inert solid propellant with 70 volume percent of particles of aluminum, potassium sulfate and ammonium sulfate, embedded in a lightly-crosslinked HTPB binder. The size of particles ranges from 20 microns to 200 microns. Figures A1(a) and A1(b) show a typical microstructure of the propellant.

The behavior of filled rubber has been studied extensively over many years (e.g., Farris 1968, 1983; Schapery 1974, 1982, 1986, 1991b) . Vacuole formation and growth (Farris 1968), the Mullins' effect (Mullins 1969), viscoelasticity (Schapery 1982), strain softening (Swanson and Christensen 1983), thermal-mechanical interaction (Hufferd 1980), finite deformations (Simo 1987, Peng 1985) all contribute to the complex behavior of filled rubber. Material damage in particulate composites arises primarily due to microcracks or microvoids forming and growing within the matrix or along the particle-matrix interfaces. Since the energy stored in a material body dissipates as damage occurs, it is reasonable to expect that the amount of energy absorbed by a body (apart from viscoelastic dissipation) should be an indicator of the state of damage of the body. In addition, it was observed that for limited strain histories the

applied work for processes in which changes in structure occur is in· ·endent of the history when viscoelastic effects are negligible. Schapery applied the concept of energy dissipation as the measure of damage and the observed phenomenon of limited path independence of work to describe the behavior ` particulate- and fiber-reinforced composites (1991b, 1989, respectively), and formalized these ideas as a general theory applicable to characterizing and predicting the mechanical behavior of elastic media with growing damage and other structural changes (1990). A brief review of the time-independent theory is presented below in order to clarify the significance of "limited path independence."

Theory

A basic assumption of the constitutive theory is that a strain energy density function $W = W(q_j, S_m)$ exists, based on thermodynamics, such that

$$Q_j = \frac{\partial W}{\partial q_j} \tag{1}$$

where,

$q_j (j = 1, 2, \ldots, J)$:	generalized displacements
$Q_j (j = 1, 2, \ldots, J)$:	generalized forces (work conjugates of q_j)
$S_m (m = 1, 2, \ldots, M)$:	internal state variables or "structural parameters"

Then, by the chain rule,

$$dW = \frac{\partial W}{\partial q_j} dq_j + \frac{\partial W}{\partial S_m} dS_m \tag{2}$$

Substituting (1) into (2),

$$dW = Q_j dq_j + \frac{\partial W}{\partial S_m} dS_m \tag{3}$$

Integrating (3) from an arbitrary state-1 to another arbitrary state-2,

$$\int_1^2 dW = \int_1^2 Q_j dq_j + \int_1^2 \frac{\partial W}{\partial S_m} dS_m \tag{4}$$

or,

$$W(2) - W(1) = [W_T]_1^2 + \int_1^2 \frac{\partial W}{\partial S_m} dS_m \tag{5}$$

where, $[W_T]_1^2$ denotes total work put into the material element during the process between state-1 and state-2. Assume that a state function $W_s = W_s(S_m)$ exists such that

$$-\frac{\partial W}{\partial S_m} = \frac{\partial W_s}{\partial S_m} \qquad \text{when } \dot{S}_m \neq 0 \tag{6}$$

Then, we may rewrite (5) as

$$[W_T]_1^2 = W(2) - W(1) + W_s(2) - W_s(1)$$

or, simply,

$$[W_T] = W + W_s \tag{7}$$

by taking $W(1) = W_s(1) = 0$ and letting state-2 represent the current state.

It is to be noted that (6) is similar to crack growth equation and, in fact, it represents an evolution law for finding $S_m = S_m(q_j)$. The left hand side of (6) is the available "thermodynamic force" for producing changes in S_m, while the right hand side is the required force. From (7) we deduce that $[W_T]$ is a point function of q_j for those processes in which the same set of S_m change,

$$W_T = W(q_j, S_m) + W_s(S_m) \;=\; W\{q_j, S_m(q_j)\} + W_s\{S_m(q_j)\}$$

i.e.,

$$W_T = W_T(q_j) \tag{8}$$

Also, by definition of work,

$$W_T = \int Q_j dq_j \tag{9}$$

From (8) and (9),

$$Q_j = \frac{\partial W_T}{\partial q_j} \tag{10}$$

That is, the work W_T is not only a state function of q_j and S_m but it is a potential function of q_j alone, thereby justifying the term "work potential." Namely, the body exihibits hyperelasticity for each set of histories $q_j(t)$ that produces structural changes defined by the same set of parameters. Equation (10) also implies that during a damage-inducing process the incremental stiffness matrix of the body is symmetric. Conversely, given that the incremental stiffness matrix is symmetric during a damage-inducing process, it has been shown that both equations (6) and (10) follow. Either equation (1) or (10) may be used in characterizing or predicting mechanical behavior of an elastic body undergoing structural changes.

One of the primary goals of this project was to extend the existing elastic model to incorporate measured effects of viscoelasticity and temperature, starting with the simplified model developed previously (Schapery, 1991a). Specifically, the explicit forms of the material constitutive functions which depend on structural parameters, S_m and time, t are being sought. In order to experimentally characterize the isochronal behavior of the propellant (as required by the theory), constant strain-rate test data were converted to constant-time data through cross-plotting of multiple sets of constant-rate data. Also studied was whether or

not the time-temperature superposition principle originally developed for thermorheologically simple linear viscoelastic materials is applicable to characterizing nonlinear viscoelastic behavior associated with growing damage. On the other hand, to be able to predict responses under more general multiaxial loading conditions not used in the characterization process, some means of physically meaningful multiaxial theory is required. A micromechanical model developed by Schapery (1986, 1991b) provides one such theory. In this model, a combination of perturbation and strain energy methods was used to predict the effective moduli of a highly filled particulate composites. The geometric idealization of a generalized self-consistent method was used in the analysis to develop the multiaxial theory.

Experiment

A gas dilatometer developed by professor Farris of University of Massachusetts was used to measure change in volume of the specimen under continuous axial straining and fixed confining pressure. Stresses were also measured at the same time as dilatation. Various combinations of different axial strain rates (.059%/sec, .59%/sec, 5.9%/sec, 23.8%/sec), confining gage pressures (0psi, 75psi, 200psi, 800psi), and temperatures (25C, -10C, -25C, -40C) were applied (see Table A1). For each combination of test paramaters, typically five specimens were tested for development of average properties. Significant specimen-to-specimen variation was observed due to the intrinsic inhomogeneity of the bulk material. An Instron universal testing machine together with a Bemco environmental chamber were used to provide axial straining and controlled temperatures, respectively. Compressed dry Nitrogen gas was used to provide confining pressures. An automated data acquisition system on a personal computer was employed. A typical test setup and a specimen configuration are shown in Figure A2. A series of similar tests without pressure were performed previously using a liquid dilatometer based on a design developed by the Navy Weapons Center (see Figure A3). The liquid dilatometer was not appropriate for tests with confining pressure, and the accuracy of dilatation measurements was not as good as the gas dilatometer. JANNAF Class-A uniaxial specimens were cut out of material blocks using a die-cutter and their ends were glued to aluminum tabs using ployurethane adhesives.

Some typical responses are presented in Figures A4(a) through A4(c). Figure A4(a) shows strain-stress-dilatation behaviors under various fixed strain rates and fixed temperature and confining pressure. It is seen that the stress increases as the strain rate increases just as in simple linear viscoelasticity. The dilatation, which is an indicator of the degree of material damage, generally increases with increasing strain rate. It seems, however, that a threshold value of strain rate exists such that when a strain rate smaller than the threshold value is

applied the dilatation may increase with decreasing strain rate. The currently available data, however, are not sufficient to confirm this hypothesis. Tests at strain rates lower than the currently lowest rate were not possible due to the inherent limitations of the dilatometer. Figure A4(b) shows the responses under various fixed pressures with fixed temperature and strain rate. The axial stress increases with increasing confining pressure, but the dilatation decreases with increasing pressure. It is understood that high confining pressure retards vacuole formation and effectively prevents significant material damage from taking place. In Figure A4(c) material behavior under various fixed temperatures with fixed pressure and strain rate are shown. The material becomes stiffer and experiences more damage at each strain as the temperature decreases at a fixed strain rate.

T= 25C (Room Temperature)

strain rate / pressure	.059 %/sec	.59	5.9	23.8
0psi	X	X	X	X
75	X	X	X	X
200	X	X	X	X
800	X	X	X	X

T= -10C

strain rate / pressure	.059 %/sec	.59	5.9	23.8
0psi	X	X	X	X
75				
200		X		
800				

T= -25C

strain rate / pressure	.059 %/sec	.59	5.9	23.8
0psi	X	X	X	X
75				
200		X		
800				

T= -40C

strain rate / pressure	.059 %/sec	.59	5.9	23.8
0psi	X	X	X	X
75				
200				
800				

Table A1 Executed Combinations of Test Parameters

(a)

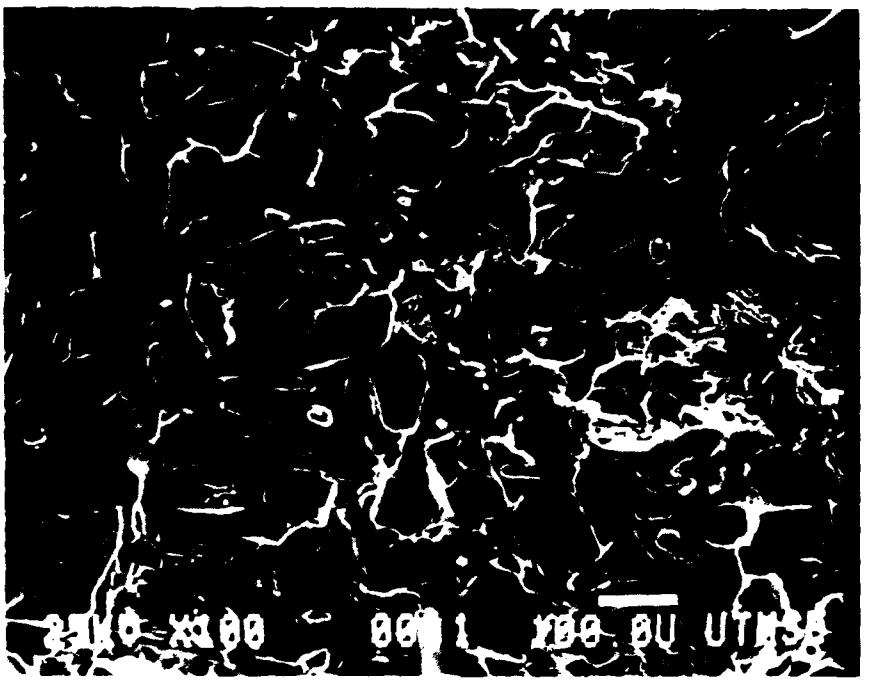

(b)

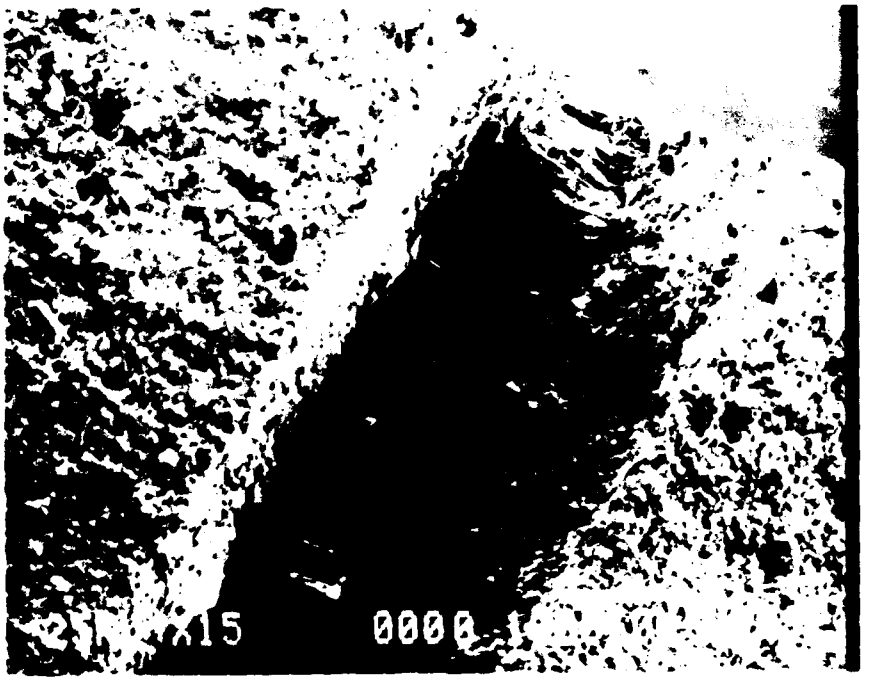

Figure A1 Visual Observation of Inert Solid Propellant through SEM
(a) View of Knife-Cut Surface (x300)
(b) View of Macro-Crack Edge (x15)

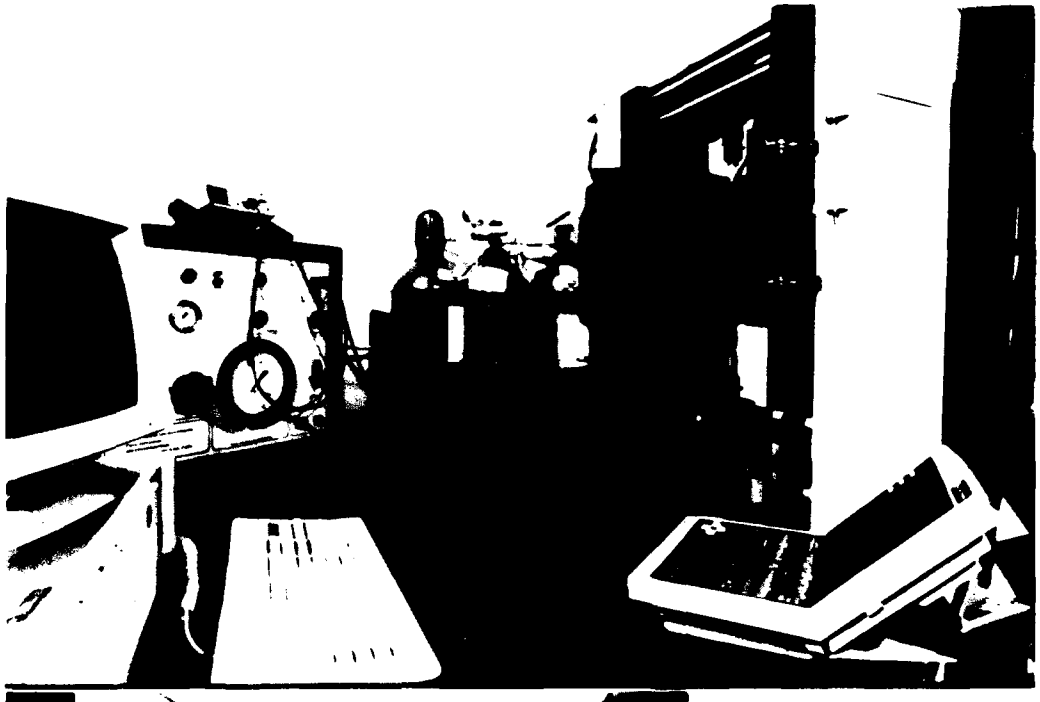

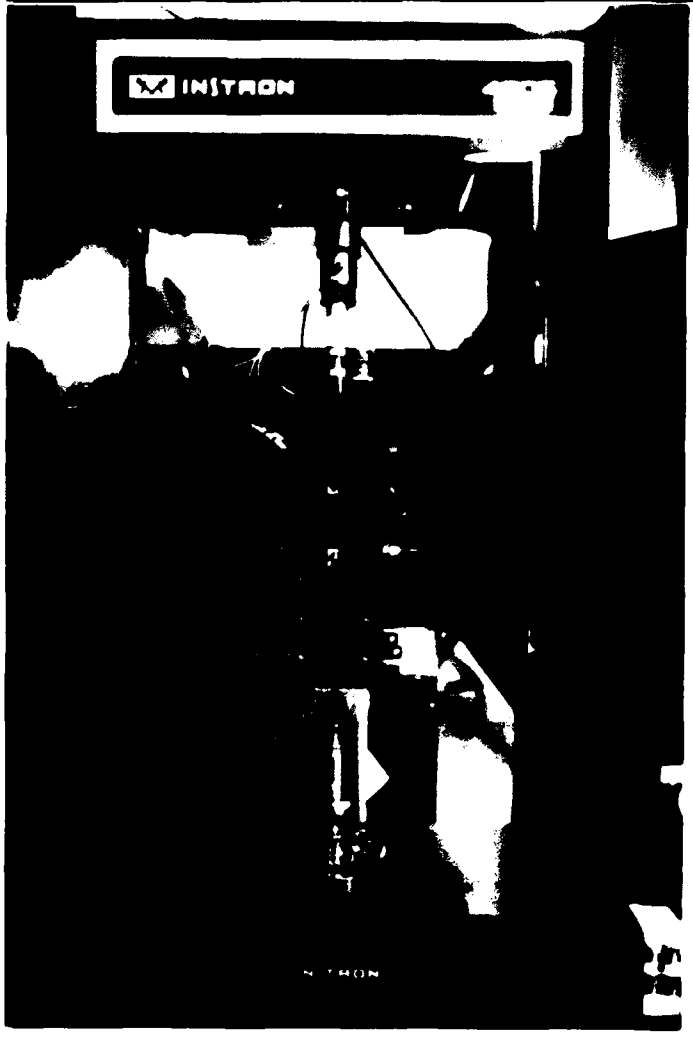

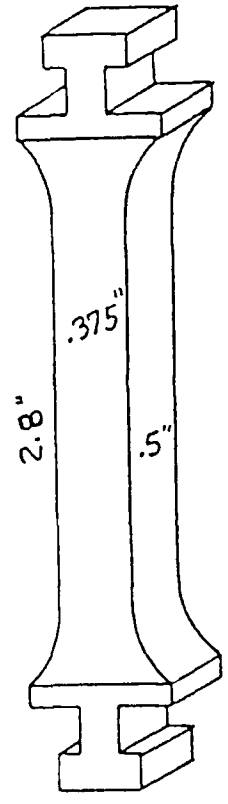

JANNAF "class-A" Type

Figure A2 Gas Dilatometer Test Set-Up and Specimen Configuration

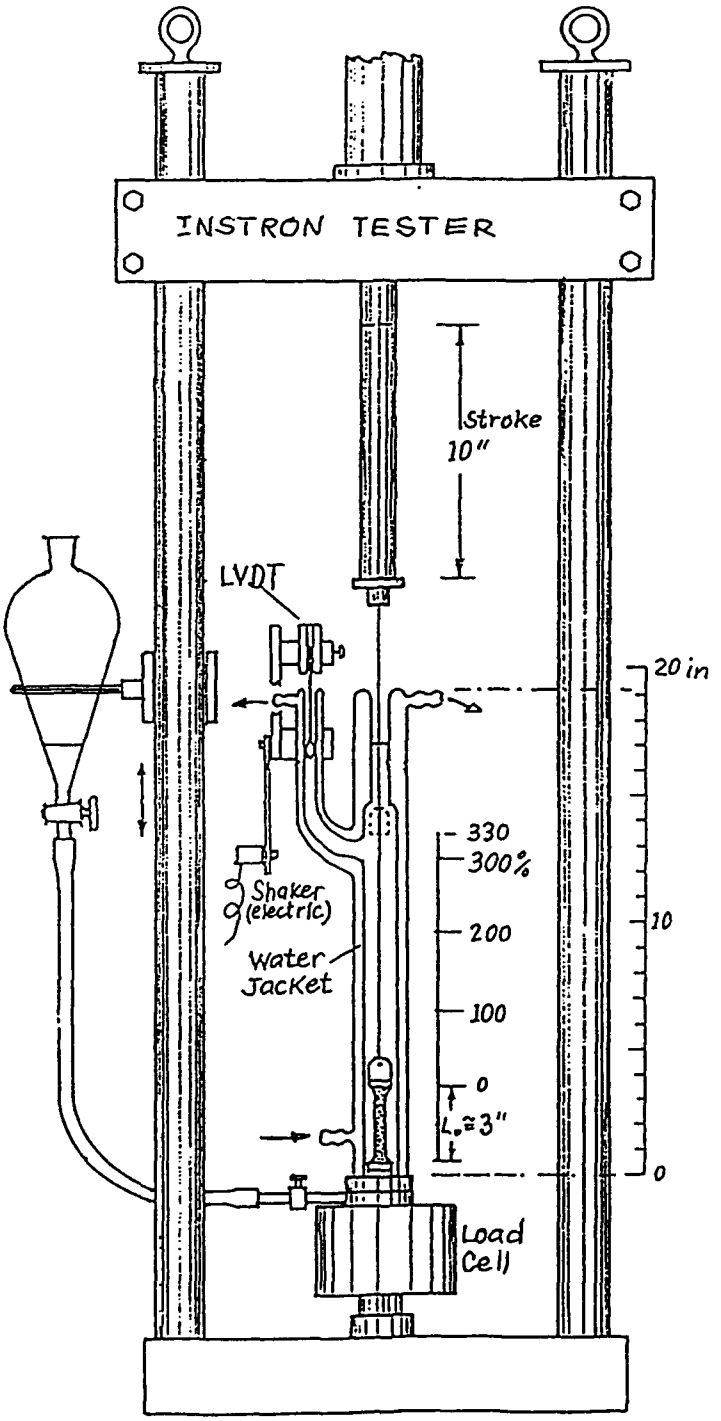

Figure A3 Liquid Dilatometer Test Set-Up

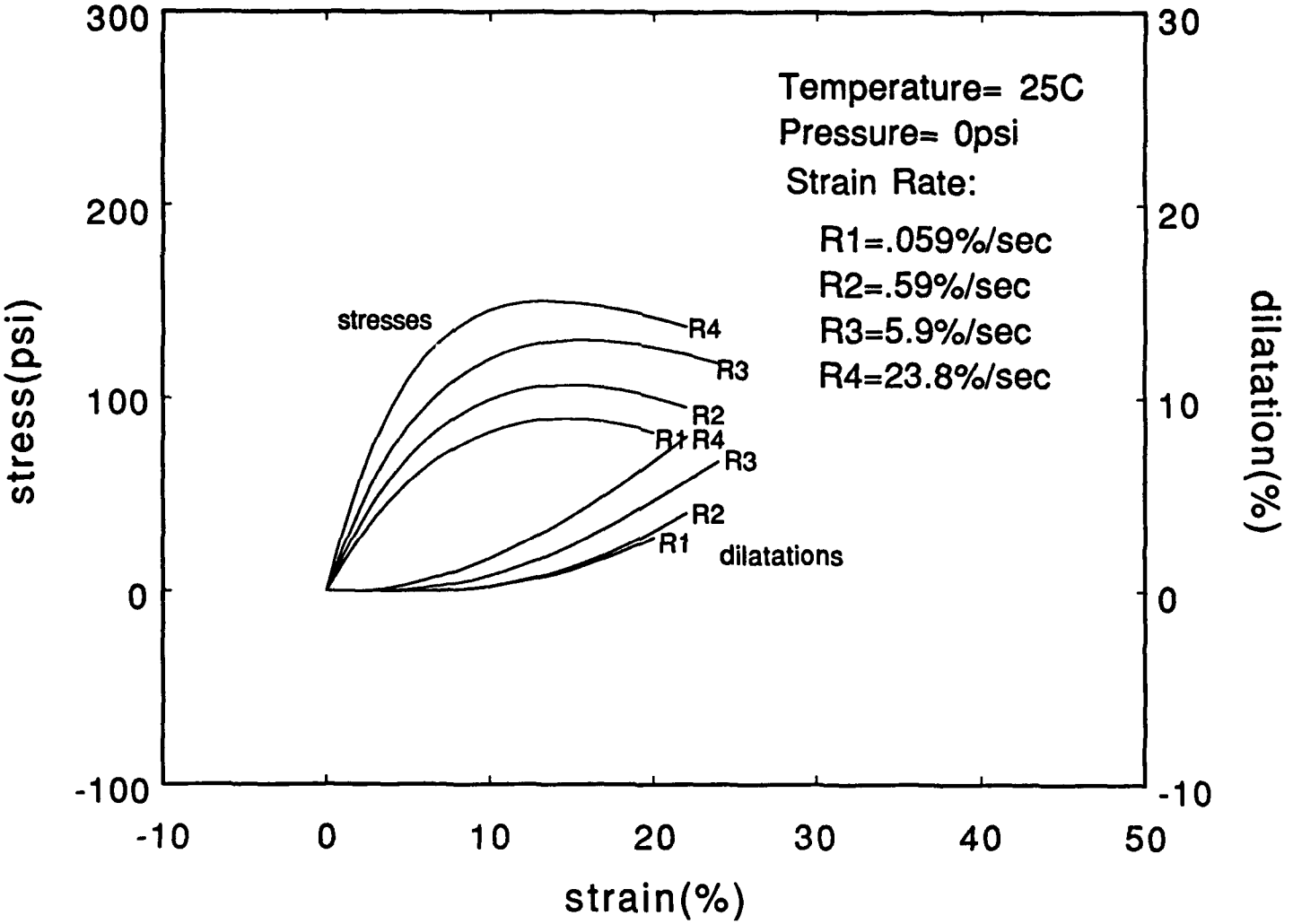

Figure A4 Typical Stress-Strain-Dilatation Response of Inert Solid Propellant (a) under Fixed Temperature, Fixed Confining Pressure, Varying Strain Rate

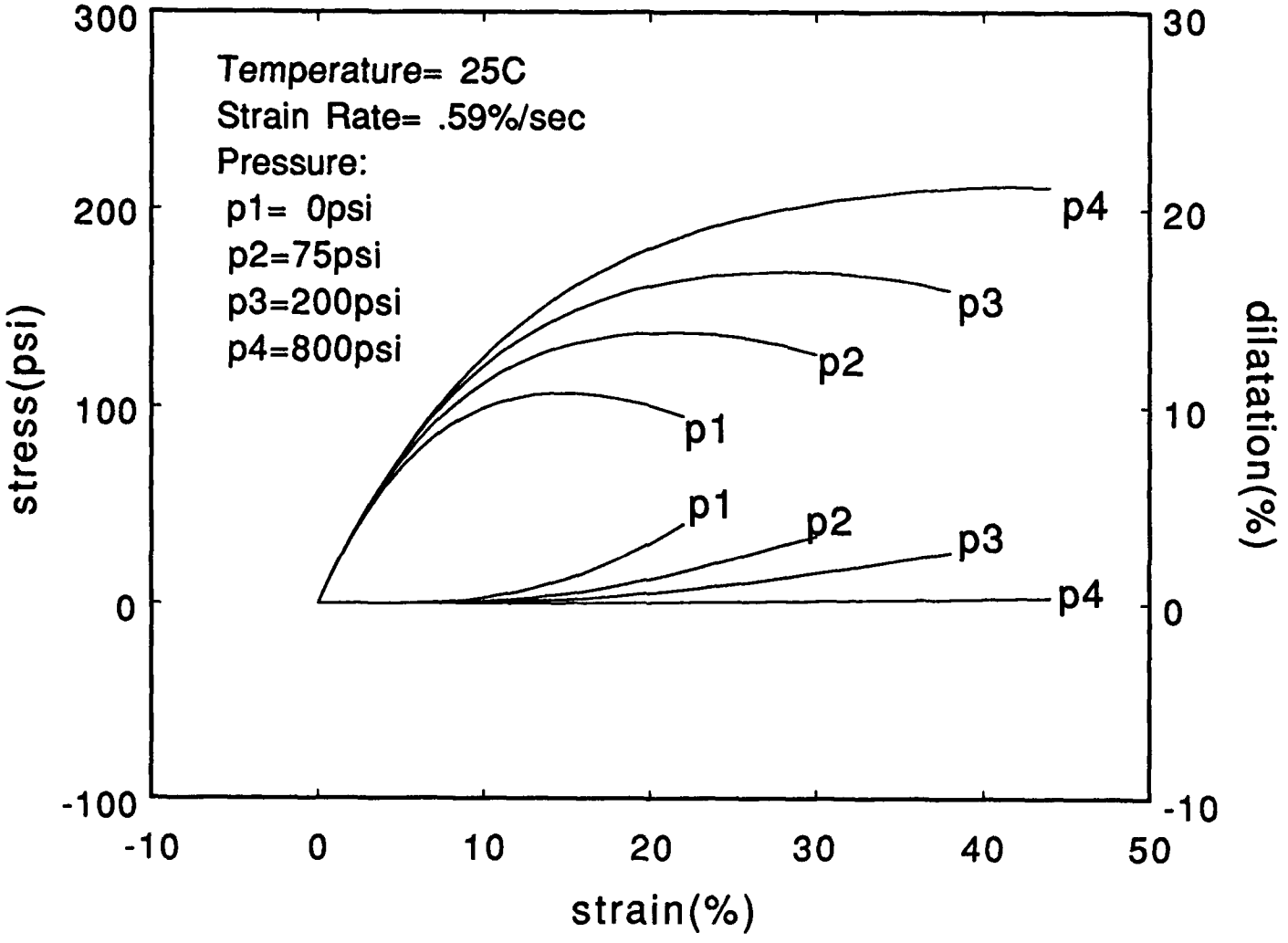

Figure A4 (continued)
(b) under Fixed Temperature, Fixed Strain Rate, Varying Confining Pressure

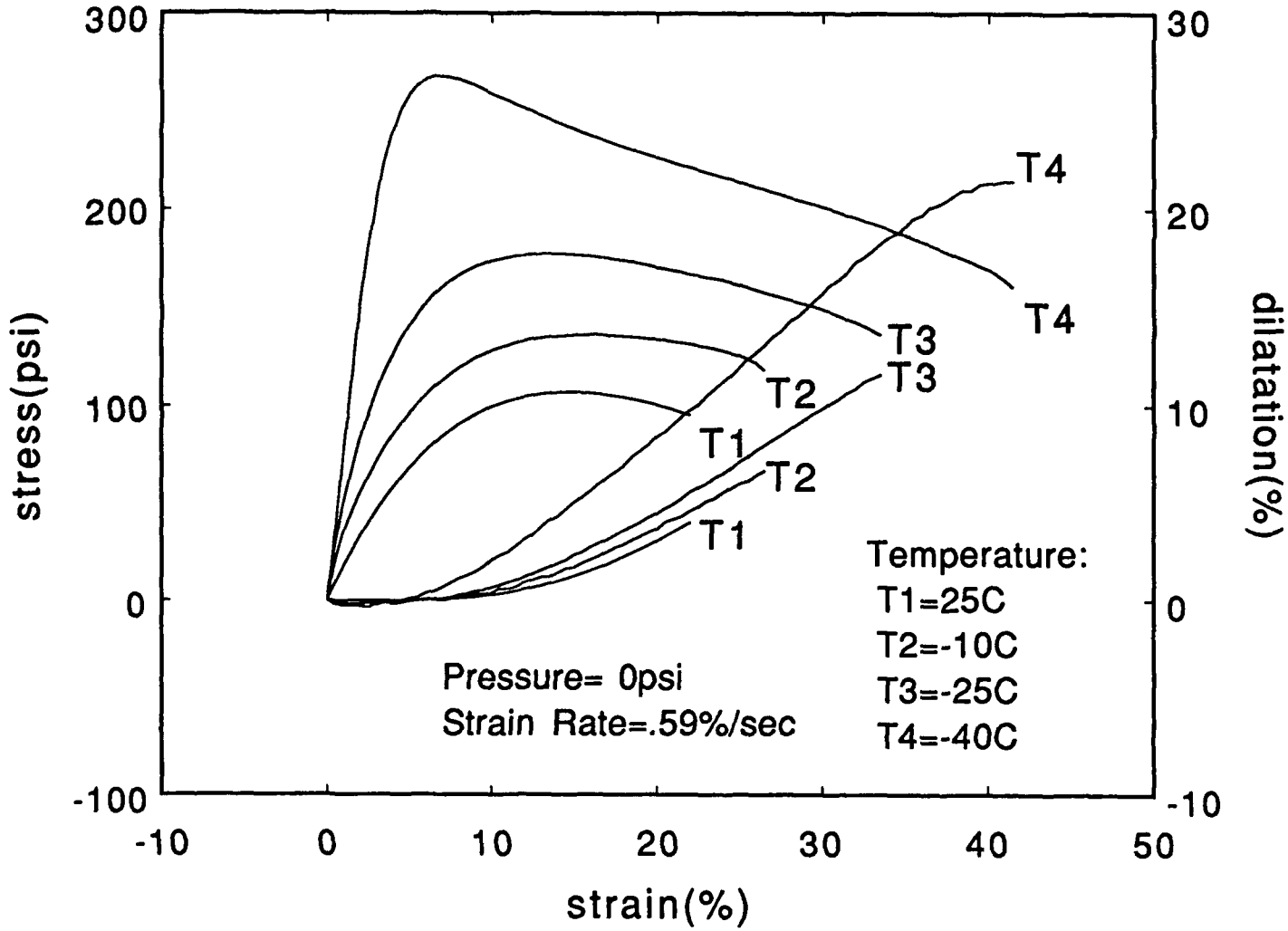

Figure A4 (continued)
(c) under Fixed Pressure, Fixed Strain Rate, Varying Temperature

APPENDIX B

Macrocracking in a Composite with Distributed, Growing Damage

Introduction

When macrocracks occur in rocket motor grains, they may significantly alter the safety and motor performance. Over the years, attempts have been made to develop mathematical models for predicting crack growth behavior, but the validation was limited due to the lack of the experimental data base and nonlinear theory. In particular, the near-tip behavior of material around cracks in solid propellant during crack opening and extension needs to be quantified analytically and experimentally.

Choice of Experimental Method

Whole-field optical methods potentially applicable for deformation measurements include speckle, moiré , grid and digital image correlation methods. The first two techniques have limitations in two respects. First, they have stability requirements, that is, rather large rotations and strains cause ambiguous results in the near field around the crack tip. Secondly, the data processing required to reduce the fringe patterns into desired data is laborious and time-consuming. Here, we consider the grid method first for the in-plane displacement measurements, and later we describe digital image processing method (which overcomes problems with the grid method).

Preparation of Propellant Test Specimens

Conditions for each test are listed in Table B1. Most specimens we have used are made of inert solid propellant consisting of a rubber matrix filled with hard particles, as described in Appendix A. Silicon rubber specimens were used in tests 6 and 7 in order to check the experimental method. The biaxial test specimen configuration is as shown in Figure B1. Normal sizes of the specimen were 1 inch by 6 inches with thickness of 0.5 inches, except test 5 in which we used a 4 inch by 1 inch by 0.5 inch specimen without a crack. These biaxial test specimens were bonded to aluminum grips using urethane adhesive, with 24 hours of curing time before being connected to the cross-head of the Instron test machine.

(a) Grid Method:

A grating consisting of squares 0.2 mm on a side (125 lines/inch) was applied to the specimen using the following procedure: Apply a thin layer of vacuum grease on the specimen. A screen made of thin nickel (thickness of 0.0001 inch) was pressed onto the grease. Titanium dioxide was sprinkled onto the surface. When the screen was peeled off, the powder was left stuck to the grease in clear square dots.

(b) Image Correlation Method:

We have made two tests with a silicon rubber specimen. One was without any patterns on the surface of the specimen, while the other had randomly located titanium dioxide powder on the surface.

Experimental Set-Up

The experimental set-up for solid propellant and for silicon rubber were slightly different, as depicted in Figure B2 and Figure B3, respectively. An Instron testing machine (100KN capacity) controlled by an external computer was used for both cases.

(a) Grid Method (Figure B2):

Cannon L1 camcorder(410,000 pixels CCD) was used to record the deformations on the specimen during the experiment. During the playback on a VCR (Sony model EVO-9500), the desired frames for both undeformed and deformed pictures were chosen and then freeze-framed (Kodak video printer) to print out on negative film. The negatives were magnified and developed up to about 15 times. Here we used a digitizer for manual digitization and software from VPI & SU. A flat bed scanner was employed to digitize the pictures into computer files. The NIH image 1.41 software was used in digitizing the grid intersection points.

(b) Image Correlation Method (Figure B3):

In order to minimize errors involved in printing in negatives and manual digitization, the frame-grabber board was used to translate the picture into 640 × 480 pixels (picture element) 8-bits gray scale map. The digitized image files were sent to the VMS/VAX cluster in which image processing software called IDL (Interactive Data Language) accomplished the correlation process.

Test Procedures

(a) Grid Method:

Numerous preliminary tests were conducted to establish the experimental technique. Subsequently, data were extracted from tests outlined in Table B1. The test data analysis technique was improved from test-to-test. The first four tests were mainly analyzed for the displacement and strain fields using the same technique developed at VPI & SU (D. Post and C.W. Smith, 1987). A magnified print (Figure B4) was fixed to a digitizing table used to measure the x,y coordinates of the grid intersection points. After digitization manually, the data for each grid intersection point were stored in computer memory files, viz., the column and row numbers that identify the point and the x and y coordinates of the point. Computer programs were used to perform several operations, which included four-point averaging of displacement and calculation of the strain fields as well as contour plotting.

(b) Image Correlation Method:

Normalized cross-correlation is a pattern matching technique and is a very effective method for locating patterns within an image. When running correlation, the searching area represented by a center location is stepped through the deformed configuration to find the best match within the searching area. When the best fit is found, results are saved in terms of x, y location of the match and the normalized correlation coefficients. IDL allowed us to construct contour maps of the displacements automatically , so that the physical significance of the results could be readily seen.

Test Results

(a) Grid Method:

Figure B4 is the representative print for digitization. Figures B5 and B6 are the experimental results, while Figures B7 and B8 are ABAQUS finite element predictions of vertical displacement and strain field respectively, from test 4 with 4.6% global strain. The vertical displacement and strain fields matched quite well with predictions from the linear finite element code, but the horizontal displacement was on the order of the resolution of the grid method; thus the results were not quite consistent even for repeated analysis for the same print. Tests 5 and 6 were dedicated to examine the large deformation around a specimen edge to verify this method with the aid of NIH image software, but the result was not satisfactory. The other problem, besides a resolution

limitation, was in the fact that this procedure needed great care or it would take many hours to repeat.

(b) Image Correlation Method:

Figure B9 is the representative result from Test 7, for which $\epsilon_0 = 5\%$. The test results showed that to improve this method it is desirable to use random painting of the titanium dioxide on the surface. On Figure B9 the solid line shows a 3-D linear finite element prediction of vertical displacement from ABAQUS and dashed line is from the image correlation method. Also shown is a displacement vector plot and horizontal displacement contour map in Figure B10. A reasonably good agreement between prediction and experiment may be seen.

Discussion

We have obtained the strain distributions around solid propellant cracks using the grid method. This would be acceptable for measurements of large deformation-induced displacement field with moderate accuracy. We compared the linear theory with experimental results. The local strain and displacement fields were not very close to the linear theory; as expected, it will be necessary to introduce the effect of distributed damage in the theory. The digital image correlation method, after more verification and calibration, is expected to give reproducible and accurate results.

Table B1. Test Conditions

Test No.	Cross-Head Speed(in./min.)	*Global Strain(%)	Interest Area	Test Material	Remark
1	0.1	4	Crack Tip	Propellant	
2	0.02	N/A	N/A	Propellant	Retest (like Test #1)
3	0.02	1·1	Crack Tip	Propellant	Grid Method
4	0.1,1,10	6	Crack Tip	Propellant	Grid Method
5	0.1	5.5,7.5,10	Edge	Propellant	4" x 1" x 0.5"
6	0.1	5	Edge	Silicon Rubber	(No Crack) Grid Method
7	0.05	15	Crack Tip	Silicon Rubber	Image Correlation

* Global strain is defined as $\varepsilon_0 = (\delta/h)$ x100%

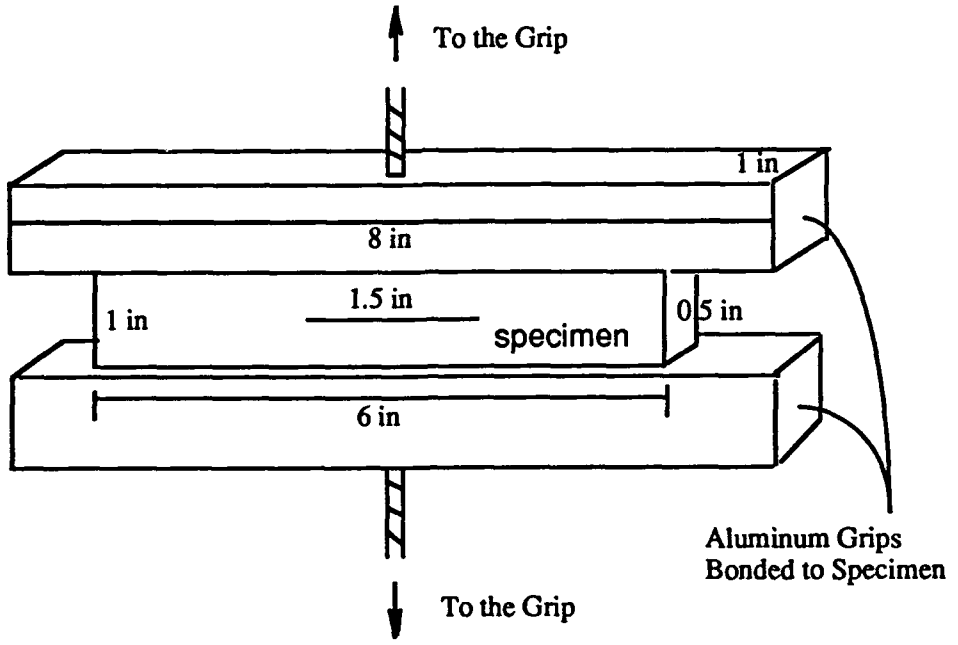

Fig. B1 Specimen Dimensions

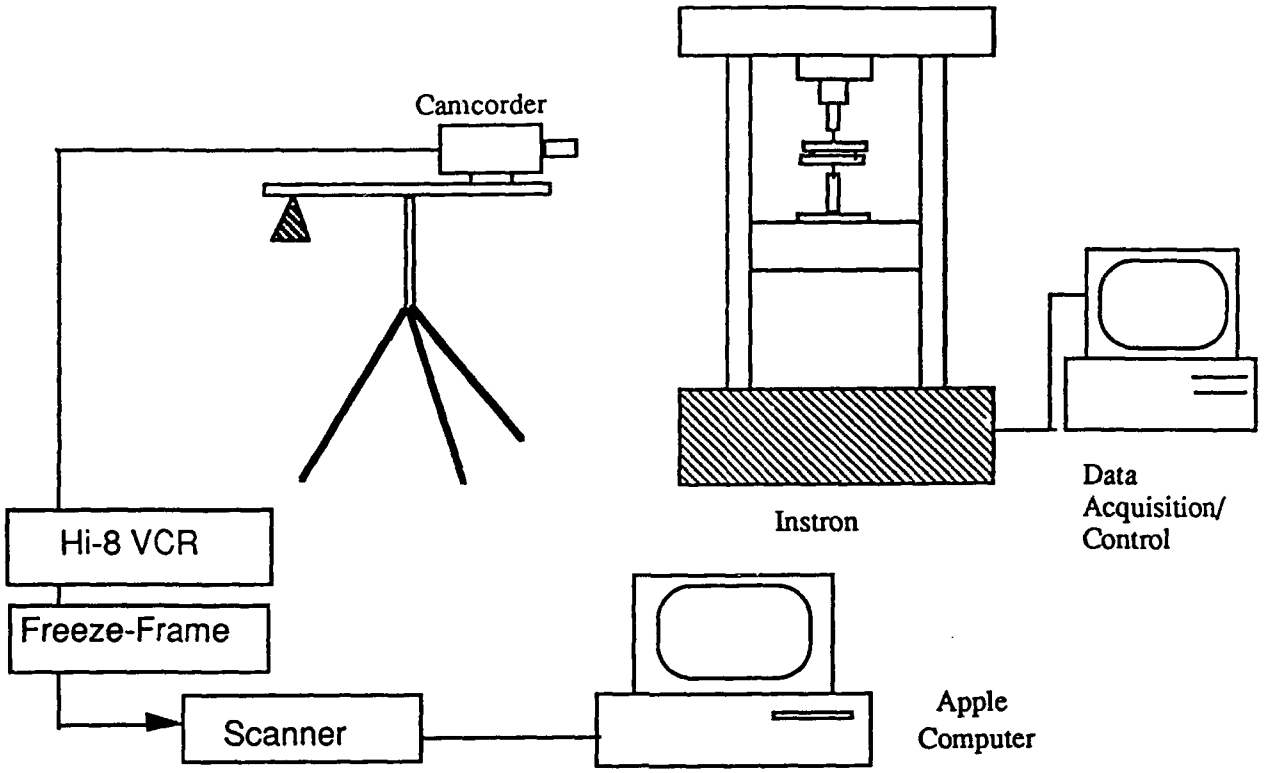

Fig. B2 Experimental Set-Up for Grid Method

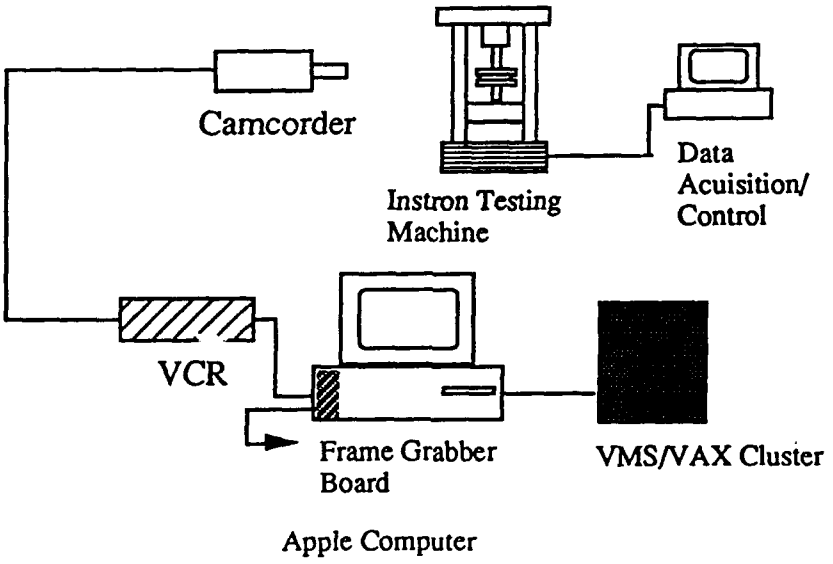

Fig. B3 Experimental Set-Up for Image Correlation Method

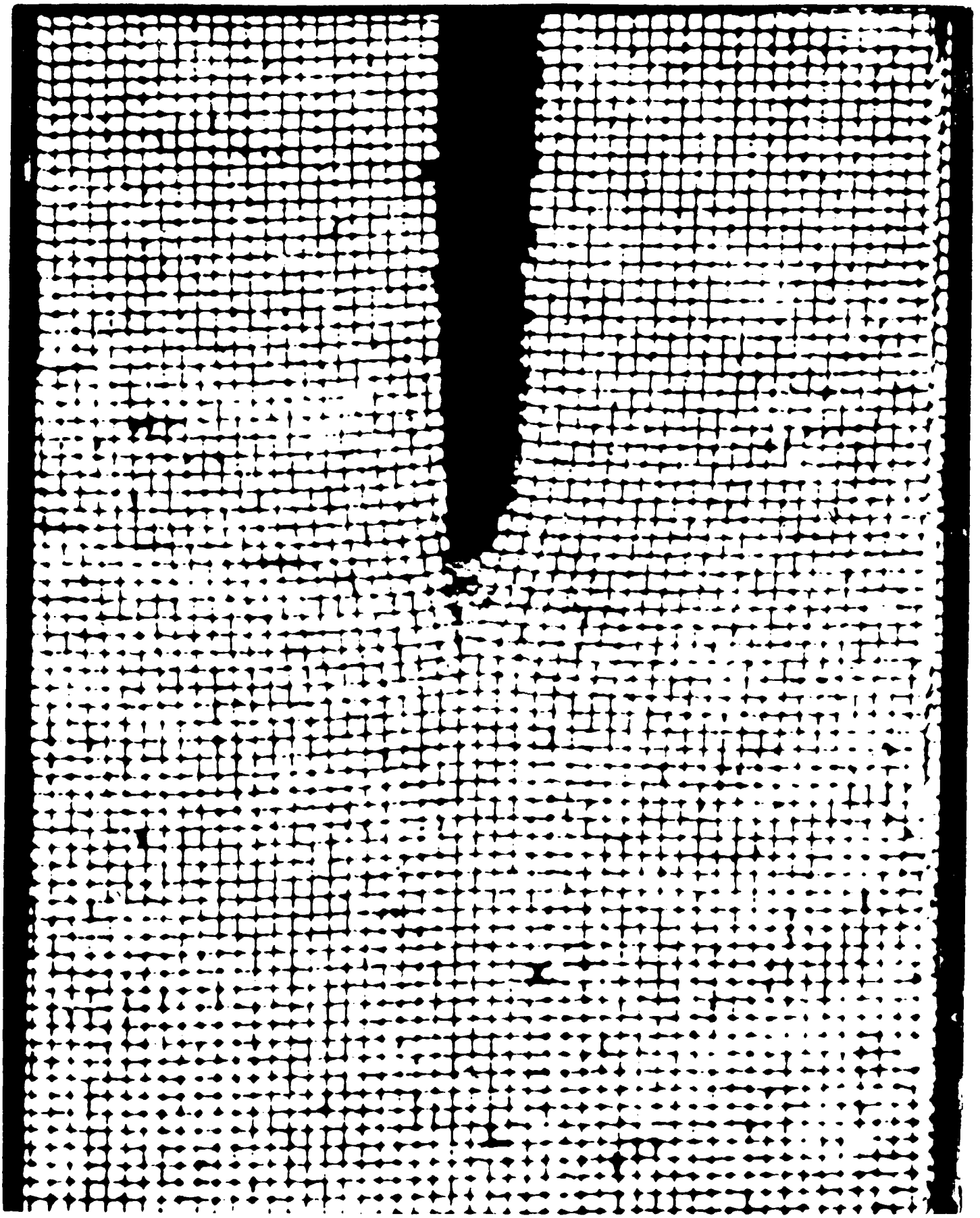

Fig. B4 Deformed Configuration with 4.6% Global Strain (Test 4)

VERTICAL STRAIN FIELD

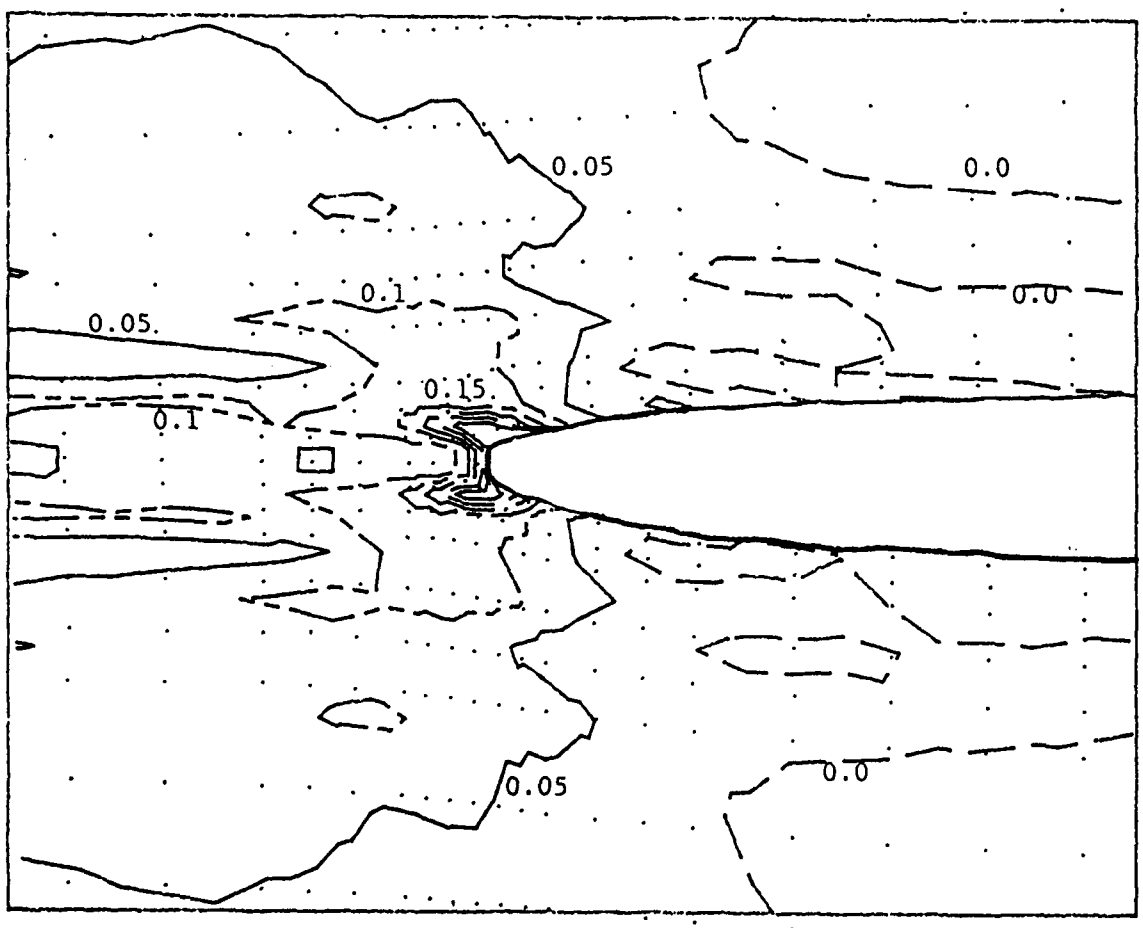

HX = 9.38927 mm

HY = 7.39315 mm

Fig. B5 Vertical Strain Field (Test4; 4.6% Global Strain)

V-DISPLACEMENT FIELD

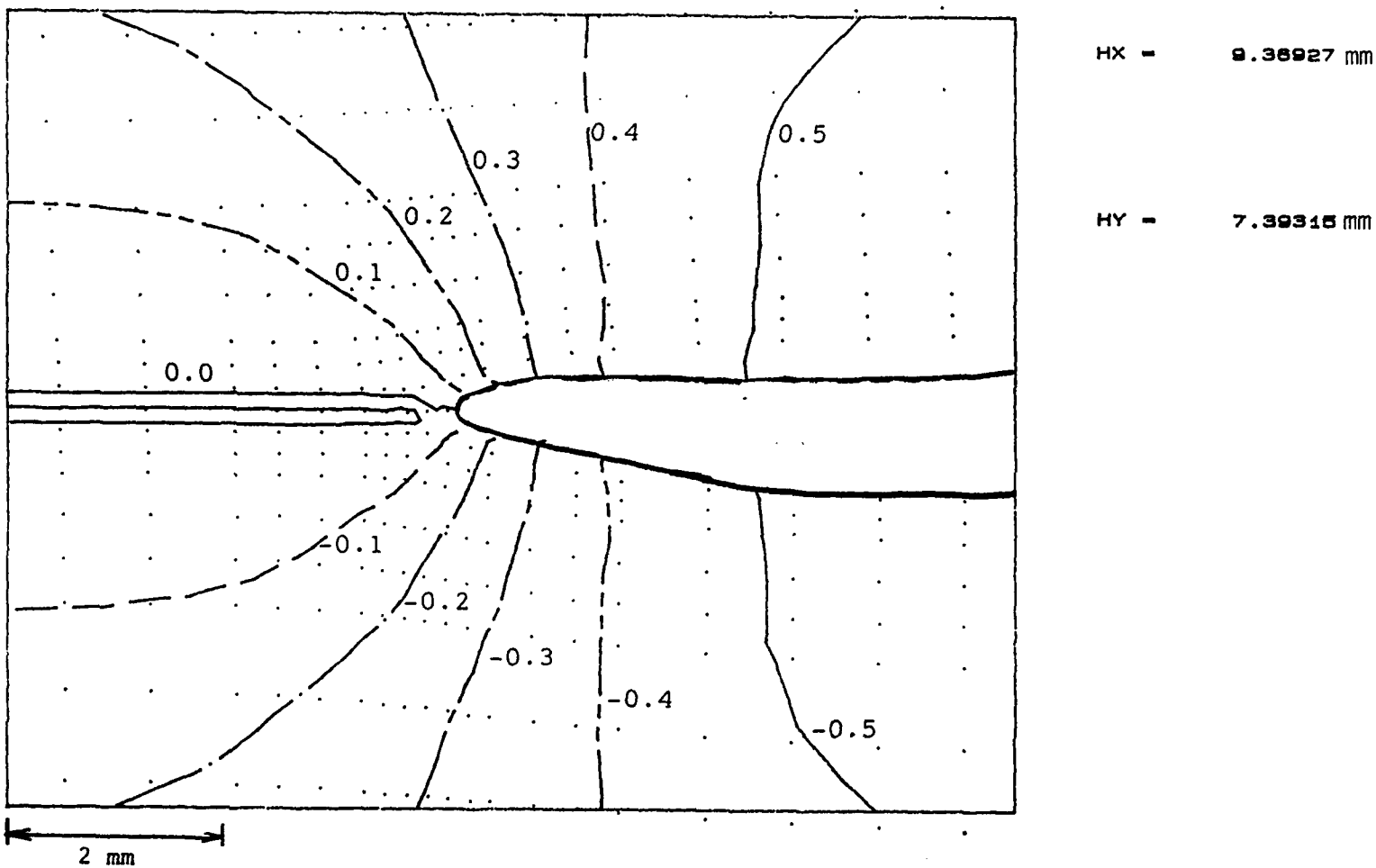

Fig. B6 Vertical Displacement Field (Test4; 4.6% Global Strain)

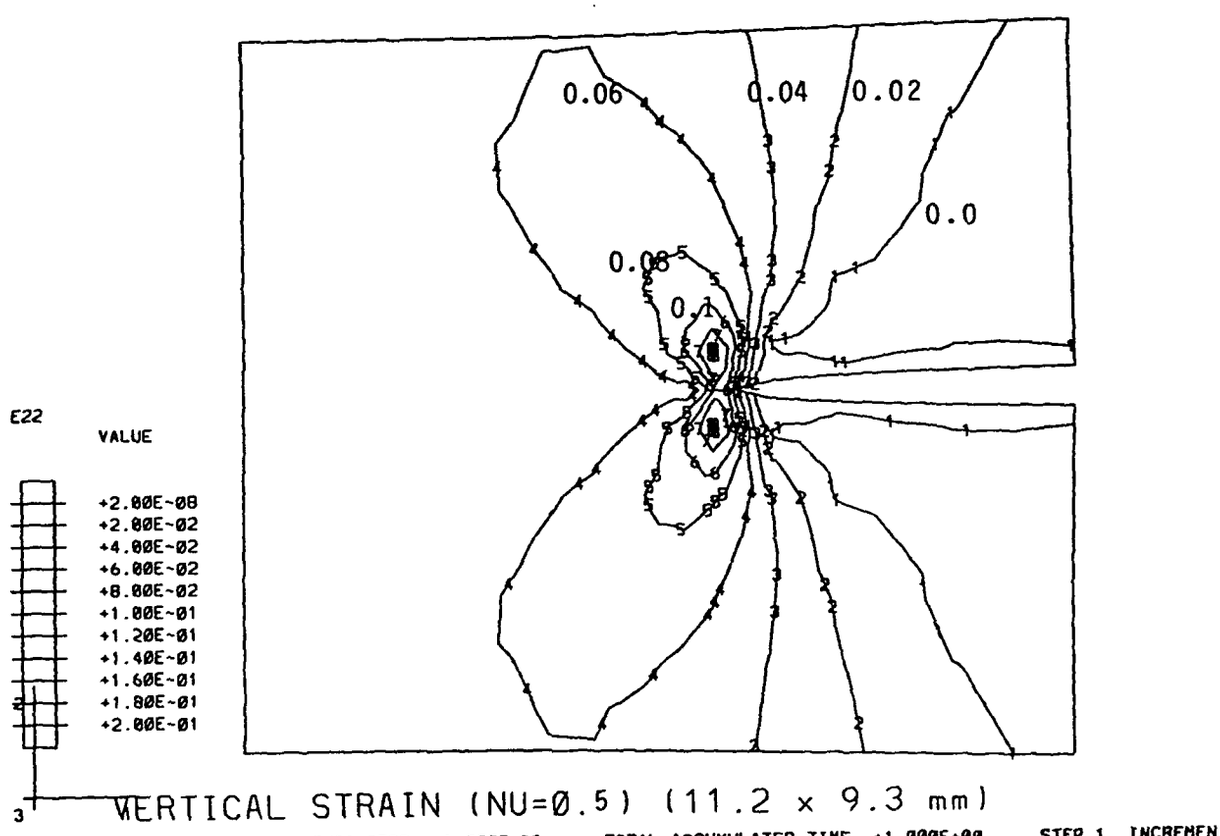

Fig. B7 Vertical Strain Prediction by
Linear Finite Element Method (5% Global Strain)

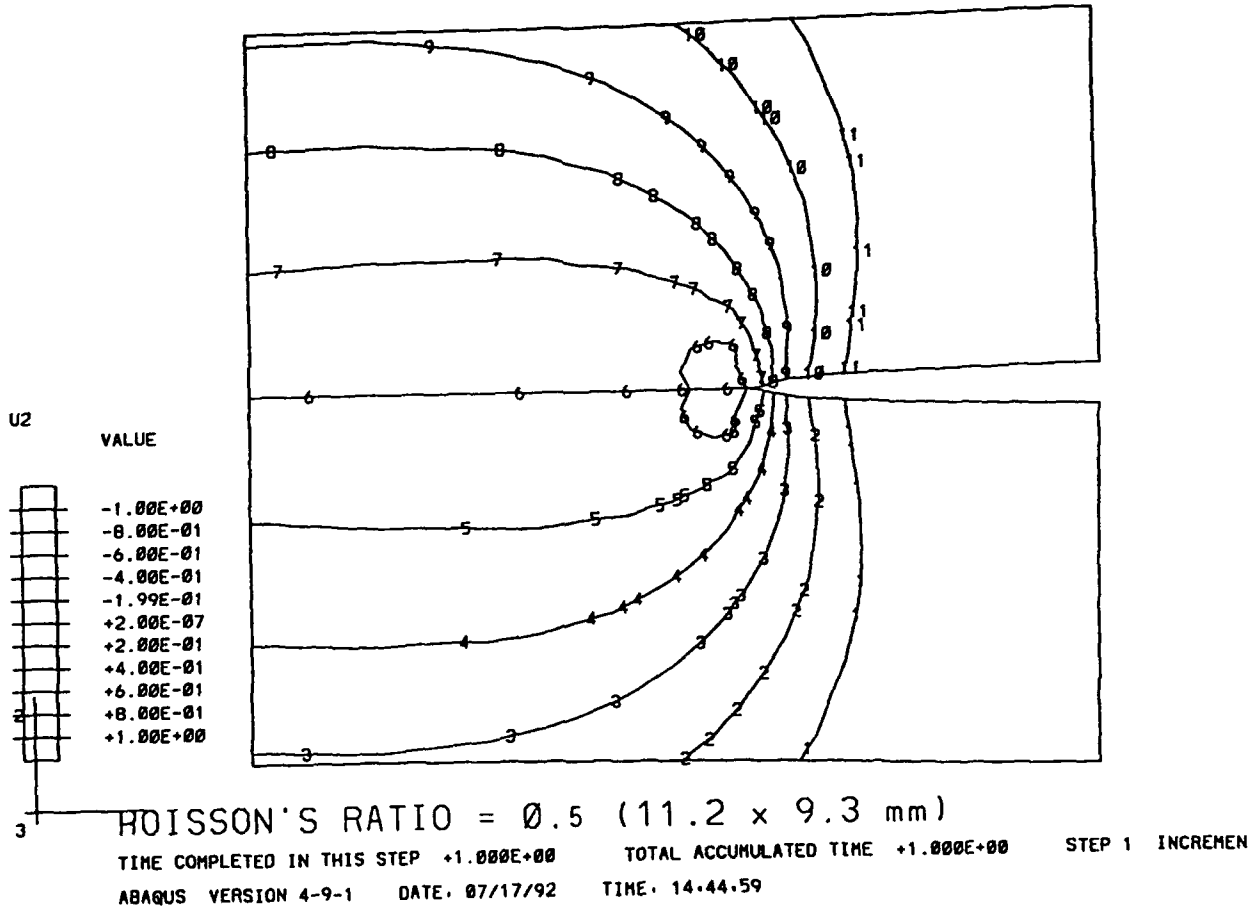

Fig. B8 Vertical Displacement Prediction by Linear Finite Element Method (5% Global Strain)

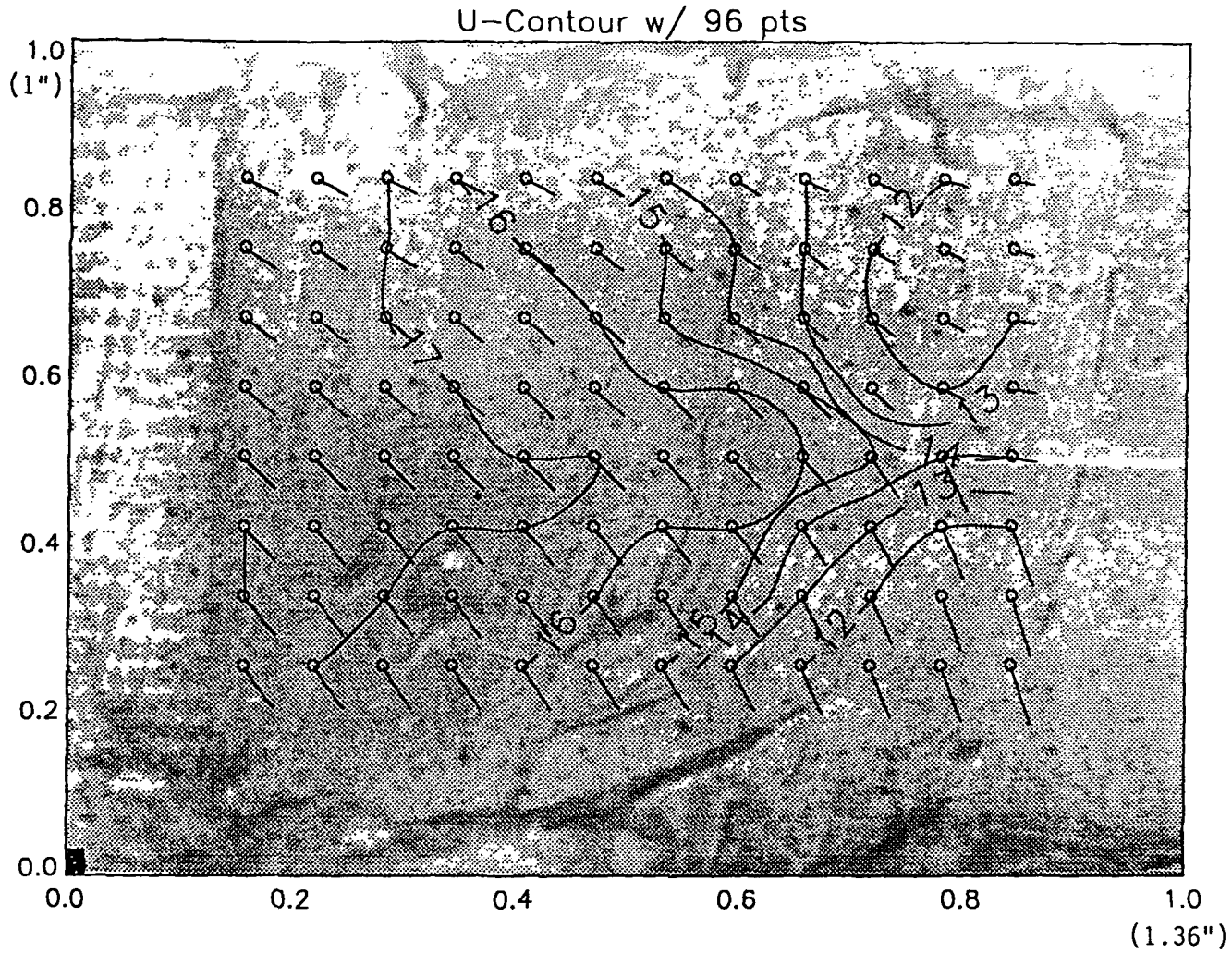

Fig. B9 Horizontal Displacement Contour Maps
and Displacement Vectors (Test7, Global Strain of 5%)

* Numbers on the contours are multiplied by 480 and the unit is inch.
(e.g., 12 = 0.025 in)

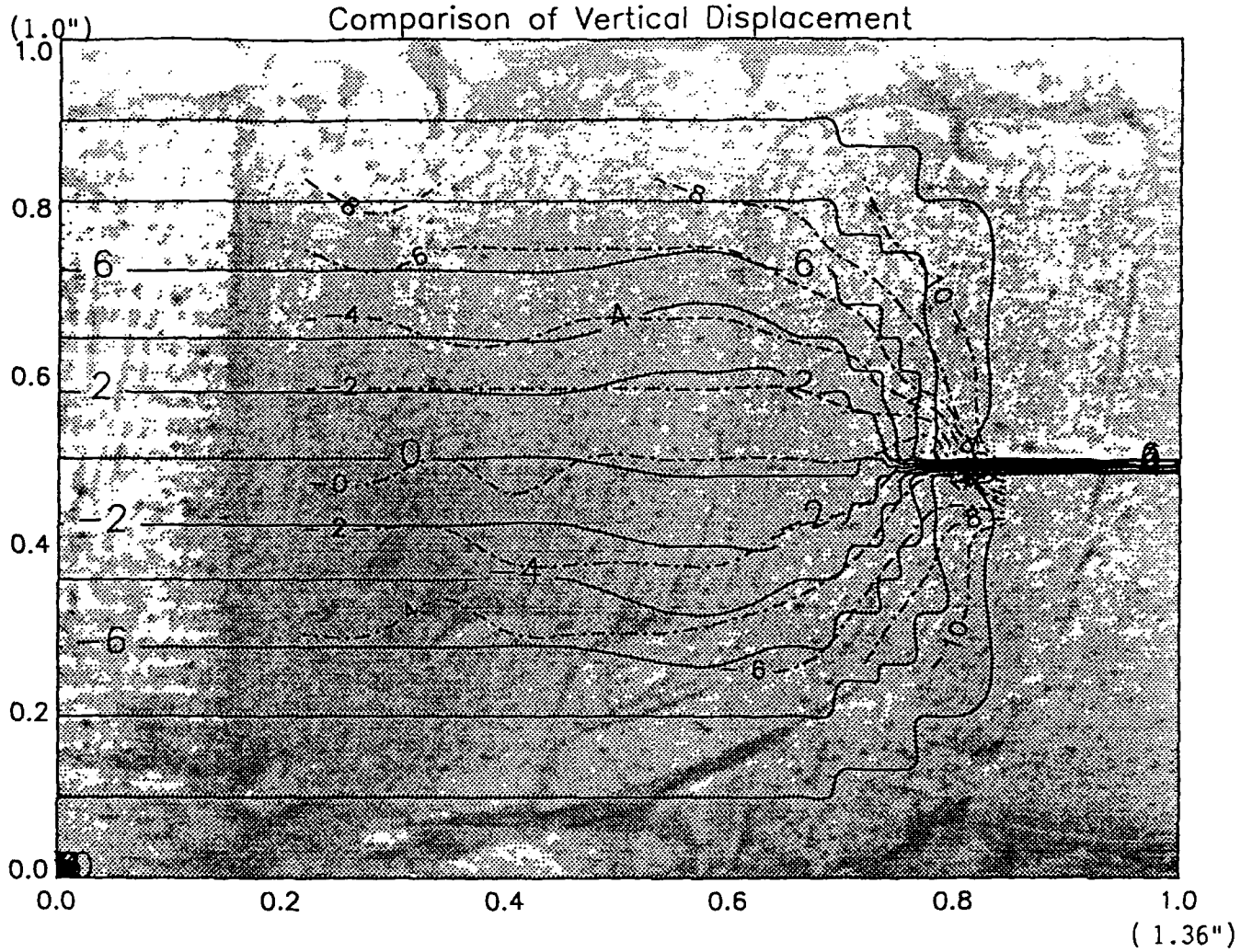

Fig. B10 Horizontal Displacement Contour Maps and Displacement Vectors (Test7, Global Strain of 5%)

* Numbers on the contours are multiplied by 480 and the unit is inch. (e.g., 12 = 0.025 in)